Journal of Structural Dynamics, 2, (pp. 105-121) 2023
On the estimation of the shear modulus of a honeycomb sandwich panel from X-ray mapping of its core.

On the estimation of the shear modulus of a honeycomb sandwich panel from X-ray mapping of its core.

Q. Leclère *[1], K. Ege[1], F. Marchetti[2], N.B. Roozen[3], Ph. Duvauchelle[1], M. Tahraoui[1], and V. Kaftandjian[1]

[1] *Univ Lyon, INSA-Lyon, LVA EA677, F-69621 Villeurbanne, France*
[2] *Matelys - Research Lab, F-69120 Vaulx-en-Velin, France*
[3] *Laboratory for Acoustics, Soft Matter and Biophysics, Department of Physics and Astronomy, KU Leuven, Celestijnenlaan 200D, B3001 Heverlee, Belgium*

Abstract

Honeycomb sandwich panels are widely used in the industry because of their outstanding stiffness to mass ratios. The dynamic response of such structures is known to be relatively complex especially in the mid-frequency domain where a strong orthotropy can be observed. Several equivalent models are available in the literature to understand and predict this behavior, all relying on an assumption that the geometry of the honeycomb core is periodic and perfectly known. The effect of imperfection inevitably introduced at the manufacturing stage are characterized in this work using X-ray measurements. A simple homogenization approach is proposed, allowing the prediction of the shearing properties of the core from statistics extracted from its geometry. These properties are used to predict the dynamic behavior of the structure using a multi-layer analytical model. Results are compared to Laser Doppler Vibrometer measurements, showing a very good agreement with the predictions based on X-ray pictures.

Keywords: homogenisation approach; X-ray pictures; honeycomb core; imperfect lattice; equivalent shear modulus; dynamical modeling; wide-frequency band; experimental validation; statistical observations; image analysis

Received on February 9, 2023, Accepted on December 4, 2023, Published on December 15, 2023

1 Context and introduction

A major industrial challenge in mechanical engineering and a hot topic of research concerns the modeling, the design and the characterisation of structures combining high rigidity with low density. Honeycomb panels are widely used for vibroacoustics applications in industry (automotive, aerospace, civil engineering...), for their high strength to weight ratio characteristics in comparison to other traditional material. The high-rigidity is obtained by offsetting the skins from the neutral axis using a thick honeycomb core layer with a very low density (constituted of hexagonal open cells, mostly in aramid papers, or thin aluminum cells...) compared to other multilayer composites structures (with homogeneous polymeric/viscoelastic core for example).

An extensive amount of literature exists on the mechanics of honeycomb structures beginning with the pioneer studies of Kelsey *el al.* [1] and Abd El-Sayed *el al.* [2], followed by the work from Gibson and Ashby [3]. The latter authors compiled a well-known *Cellular solid* book [4] (chapter 4), a reference for the community. The book gathers the theoretical approaches (*homogenisation* theories) that are required for the derivation of the in- and and out-of- plane elastic properties of hexagonal cellular cores for a given geometry. The flexural vibrations of

*quentin.leclere@insa-lyon.fr

honeycomb panels in a wide frequency range have also been continuously studied along the years, experimentally, theoretically and numerically [5, 6, 7, 8, 9, 10, 11, 12, 13, 14], highlighting the importance of the shearing deformation of the core on the global dynamical behaviour of the sandwich when frequency increases. In recent studies on the dynamics of such systems (Harkati *et al.* [15] e.g.), the design of the unit cell shape is tailored and adjusted to obtain specific performances of the multilayer in terms of equivalent stiffness. *Re-entrant* honeycomb cell cores -characterised by negative in-plane Poisson's ratio values, kown as *auxetic cells*- have also been widely studied by Scarpa *et al.* e.g. [16, 17, 18, 19], making possible improvements of bending stiffness capabilities for desired frequency bands, giving higher values of the shear modulus compared to those of a regular hexagonal honeycomb, opening new perspectives in the vibroacoustics field (isolation/damping/mitigation...).

In this context of great interest for such composites panels, an important issue the community is facing concerns the uncertainty of the key parameter: the effective global *shearing* of the core. Existing equivalent wide-band dynamic models of anisotropic composites assumes, for each of the layers, a homogeneous material with equivalent mechanical parameters [20, 21, 22, 8, 23, 24, 25, 26]. The challenge when dealing with honeycomb sandwiches is to feed such condensed model with reliable characteristics reflecting the physics of the real manufactured system. Most often, the physical parameters of the skin are well known. However, the shearing modulus of the core is usually more tricky to get. This is especially the case when using polymer cores for instance [27, 28], or when the core is not homogeneous as it is the case for honeycombs. Fitting approaches can then be used to get the equivalent shearing, exploiting the strong influence of this parameter on the mid-frequency flexural response of the panels ([29, 30, 31, 32, 33]).

We propose in this paper to estimate the anisotropic equivalent shearing modulus of the honeycomb core from the actual geometry of the cells (length of the walls, angles between the walls) assessed by using X-ray measurements. It is worth recalling here that X-ray measurements (together with ultrasonic or infrared measurements) are nondestructive solutions generally used to inspect and identify local defects, disbonds, delaminations, impact damage, internal cracks, moisture intrusion, irregularities or inhomogeneity that can occur to the very light and brittle cell core during the forming process (skin-core adhesion process in particular) of manufactured honeycomb panels [34, 35, 36, 37, 38]. For instance [38] discusses the use of X-ray techniques to investigate the effects of imperfections on the buckling behaviour of honeycomb structures. However, as far as the authors know, such radioscopy imagings on real manufactured honeycomb panels have never been exploited to directly estimate the effective shearing properties. The purpose of this work is to validate such estimations by means of vibration measurements over a wide frequency range.

The paper is organised as follows. The next section (section 2.1) is devoted to the original core shearing homogenisation approach proposed in this work. This approach allows the estimation of the anisotropic shearing properties of the core from the geometrical description of the honeycomb structure. This approach is versatile enough to be fed with a statistical description of the core geometry, making it particularly valuable for cores with imperfect lattices. In section 2.2, a methodology is proposed to assess statistically the geometrical parameters of the core of a given sample from X-ray pictures. This method is applied to a sandwich panel sample, for which a statistical description of the geometry is established. Anisotropic shearing properties are then assessed thanks to the homogenisation approach presented above. The shearing of the core is expected to have a significant effect on the mid-frequency dynamic response of the panel. The following of the paper is thus dedicated to the dynamic characterisation of the sample studied in section 2.2, in order to check the validity of the values obtained from the geometrical analysis. Section 3 presents an experimental setup based on scanning Laser Doppler Vibrometry, that allows the estimation of the flexural wavenumbers of the studied sample. Results are combined in section 3.2 with a dynamic model of the structure in order to indirectly estimate the shearing properties of the core. It is finally verified and discussed in a section 4 how the shearing properties predicted from the X-ray images are consistent with respect to the observed dynamic behavior of the sample.

2 Assessment of the honeycomb core shearing properties from X-ray pictures

2.1 Homogenization of the honeycomb core shearing properties

As explained in the previous section, the MF dynamics of sandwich panels is strongly affected by the shearing properties of the core. A simple homogenization approach is proposed in this work, based on the individual stiffness generated by each wall of the honeycomb structure. Depending upon the shearing direction, each wall of the structure is subject to shearing and bending. However, the stiffness due to bending is generally assumed to be negligible as

compared to the stiffness due to shearing [4].
Let's consider the shearing stress generated by a displacement of the upper skin along direction x, with the lower

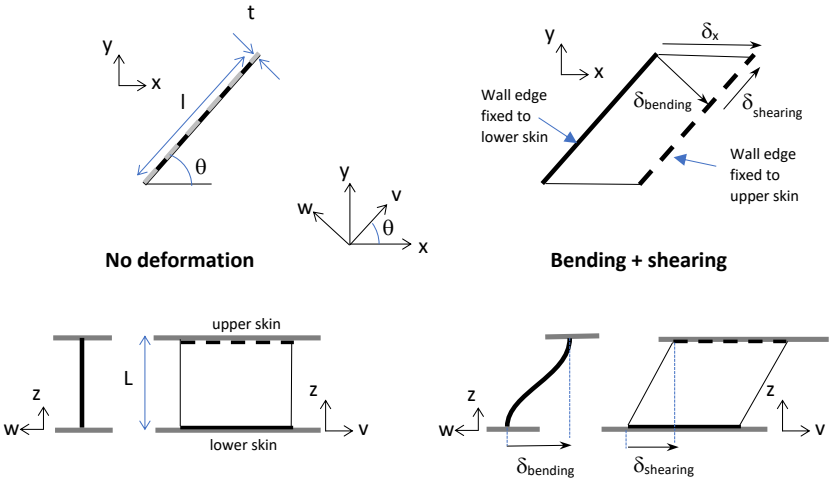

Fig. 1: Schematic representation of the deformation of a cell wall submitted to a relative transverse displacement δ_x of the skins. The cell wall is subject to bending and shearing stress depending on the angle θ between the deformation direction and the wall direction.

skin blocked (see Fig. 1). For a cell wall oriented with an angle θ regarding the strain axis x, the relative displacement of the upper and lower edges of the wall δ_x is decomposed into a displacement generated by the wall bending $\delta_{bending}$ (along w) and by the wall shearing $\delta_{shearing}$ (along v). The stiffness of the core related to the bending is neglected, because it is assumed to be negligible with respect to the stiffness related to the shearing of the wall. The boundary conditions at the junction with the skins have thus no effect. The forces generated on the x and y directions by the shearing strain along x are :

$$F_x = \frac{lt}{L} G' \delta_s \cos\theta = ltG'\gamma_x \cos^2\theta, \tag{1}$$

$$F_y = \frac{lt}{L} G' \delta_s \sin\theta = ltG'\gamma_x \cos\theta \sin\theta, \tag{2}$$

where l, L and t stand for the length, height and thickness of the wall, respectively, and G' the shearing modulus of the wall material. $\gamma_x = \delta_x / L$ stands for the shearing strain.
Let's now consider a sandwich panel with the core constituted of several walls with the same orientation θ with a given wall density equal to $1/S$ (number of walls by unit area). The in-plane shearing matrix can be defined as follows

$$\begin{Bmatrix} \tau_x \\ \tau_y \end{Bmatrix} = \begin{bmatrix} G_x & Q_{yx} \\ Q_{xy} & G_y \end{bmatrix} \begin{Bmatrix} \gamma_x \\ \gamma_y \end{Bmatrix}, \tag{3}$$

where γ, τ and G stand for shearing strain, stress, and modulus, respectively, and where Q is a coupling term between the x and y axes. Identifying these terms in Eq. 1, it becomes

$$G_x = \frac{F_x L}{\delta_x S} = \frac{lt}{S} G' \cos^2\theta, \tag{4}$$

$$Q_{xy} = \frac{F_y L}{\delta_x S} = \frac{lt}{S} G' \cos\theta \sin\theta. \tag{5}$$

where S is the surface associated to the stiffness of the wall in the homogenization process (i.e. the inverse of the number of walls by unit area).
Looking in the orthogonal direction, a similar analysis leads to

$$G_y = \frac{lt}{S} G' \sin^2\theta, \quad Q_{yx} = \frac{lt}{S} G' \cos\theta \sin\theta = Q_{xy}. \tag{6}$$

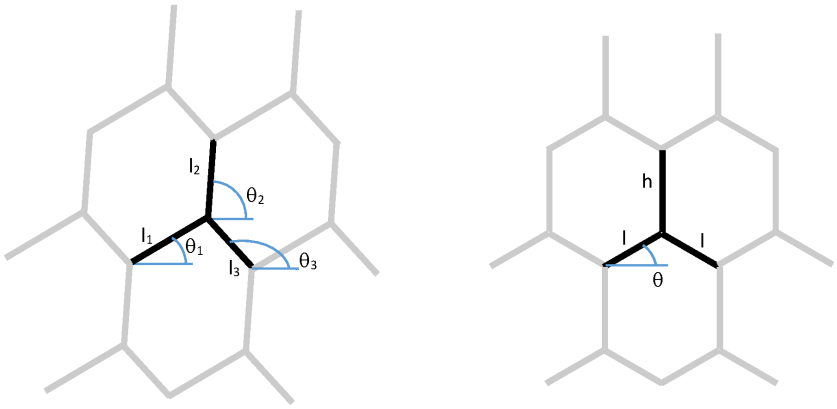

Fig. 2: Honeycomb cell structure from an Arbitrary unit cell (left). Honeycomb cell structure from a regular unit cell studied in [4] (right).

Considering a honeycomb structure constituted of a perfectly repeated unit cell, with wall lengths $\{l_1, l_2, l_3\}$, wall thickness $\{t_1, t_2, t_3\}$ and orientations $\{\theta_1, \theta_2, \theta_3\}$ (see fig 2, left), and noting S_c the surface of a cell, the homogenized shearing modulus writes

$$G_\alpha = \frac{G'}{S_c} \sum_{i=1}^{3} l_i t_i \cos^2(\theta_i - \alpha), \tag{7}$$

where α is the shearing direction (such that $G_0 = G_x$ and $G_{\pi/2} = G_y$). Note that G_α results from a linear combination of sinusoids of period π, resulting itself in a sinusoid of period π. The resulting shearing modulus G_α is consequently of orthotropic nature, that is fully characterized by the orientation of the stiffest direction, the modulus in the stiffest direction, and the modulus in the direction orthogonal to the latter (the weakest direction). It can be shown that G_α can also be written as follows:

$$G_\alpha = A\left(1 + \lambda \cos\left(2\left(\alpha - \Theta\right)\right)\right), \tag{8}$$

where

$$A = \frac{G'}{2S_c} \sum_{i=1}^{3} l_i t_i \quad , \quad \lambda = \left| \sum_{i=1}^{3} l_i t_i e^{2j\theta_i} \right| / \sum_{i=1}^{3} l_i t_i \quad \text{and} \quad \Theta = \frac{1}{2} \arg\left(\sum_{i=1}^{3} l_i t_i e^{2j\theta_i} \right).$$

The orientation of the stiffest direction is thus equal to Θ, and the modulus in the stiffest and weakest directions are $A(1 + \lambda)$ and $A(1 - \lambda)$, respectively.

Considering the coupling terms, a similar analysis leads to

$$Q_{xy} = Q_{yx} = \lambda A \sin\left(2\Theta\right). \tag{9}$$

Note that this result corresponds to a classical orthotropic behavior, the coupling term Q_{xy} being cancelled when aligning the x and y directions with the directions corresponding to the maximum and minimum values of the shearing modulus (i.e. choosing $\Theta = 0$ or $\Theta = \pi/2$).

In [4], the homogenization of the core shearing is considered for a particular unit cell satisfying $t_1 = t_2 = t_3 = t$, $l_1 = l_3 = l$, $l_2 = h$, $\theta_1 = \pi - \theta_2 = \theta$ and $\theta_3 = \pi/2$, as shown in Fig. 2 (right). In this particular case, the surface of the cell is $S_c = 2l\cos\theta(h + l\sin\theta)$ the equivalent modulus for a shearing along x ($\alpha = 0$) writes

$$G_x = G't\frac{\cos\theta}{(h + l\sin\theta)}. \tag{10}$$

The modulus along the orthogonal direction y ($\alpha = \pi/2$) is also easily obtained :

$$G_y = G't\frac{h + 2l\sin^2\theta}{2l\cos\theta(h + l\sin\theta)}. \tag{11}$$

These two expressions of the equivalent shearing modulus along x and y correspond to the upper bounds given in [4]. For the case of a perfect hexagonal cell, with identical walls ($h = l$, same thickness) we simply get

$$G_x = G_y = \frac{G't}{h.\sqrt{3}}, \tag{12}$$

that corresponds to an isotropic behavior.

However, standard honeycomb structures can exhibit strong orthotropic behaviors because of the manufacturing process. Indeed, one of the three walls of the unit structure is used to paste or bond the strips of material to each other to constite the core, as depicted in Fig. 3. This inhomogeneity induces an increased stiffness in the shearing direction parallel to the doubled walls. Considering the regular cell drawn in Fig. 2 (right), and doubling the thickness

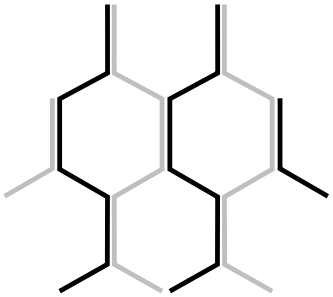

Fig. 3: Schematic structure of the honeycomb core with double-thickness walls.

of the wall of length h, Eq. 8 leads to following expressions

$$A = \frac{G't}{S_c}(l + h), \qquad \lambda = \frac{h - l/2}{l + h}, \qquad \Theta = 0. \tag{13}$$

It is worth noting that in this case the orthotropy parameter λ does not depend on θ, but only on wall lengths. In the $h = l$ case (perfect hexagone) the value of λ is equal to 1/4, and stands within 0.21 and 0.29 for h/l varying between 0.9 and 1.1 (the orthotropy increase when h/l increase). The θ parameter plays a role in the value of S_c, thus affecting the value of A.

Moreover, it is known that the actual honeycomb geometry is imperfect, which has inevitably an impact on the mechanical properties. This makes invalids the expressions for the honeycomb stiffness as derived for perfectly periodic core structures (cf. Eq. (10) and (11)).

In the following section, a method is proposed to estimate the actual mechanical properties of a honeycomb sandwich panel with an imperfect core structure, from a statistical description of the core properties as obtained from X-ray pictures.

2.2 Estimation of the orthotropy features of the core shearing from observed geometrical properties

In the previous section, a simple homogenisation approach has been proposed to estimate the in-plane shearing properties of a honeycomb core, separating the shearing stress contributions of the three cell wall families. This simple approach has the advantage of being also applicable to cell wall lengths and orientations estimated from a real structure: instead of being summed over wall families as in Eq. (7), the shearing modulus will be summed over the whole set of cell wall properties obtained from X-ray data of a given sandwich panel.

The studied plate is the same as the one used in [32]. It is made of two aluminium skins separated with a Nomex honeycomb core. The thickness of each skin is 0.6 mm while the thickness of the core is 9 mm. The dimensions of

the sample are 0.73×0.52 m^2.

The honeycomb-sandwich sample has been tested with a X-ray radioscopy imaging setup as shown in Fig.4. The

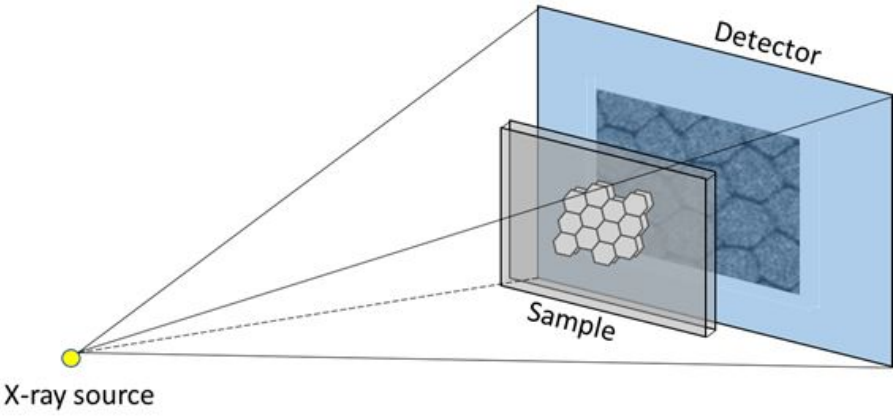

Fig. 4: X-ray radioscopy imaging setup.

radiation source is a standard industrial X-ray source with a 3 mm mini focus and the detector is a flat panel with a 200×200 μm^2 pixel size. The source to detector distance is set at 2050 mm and the sample is positioned against the detector so that the magnification is close to unity with a very small geometrical unsharpness around 7.5 μm. The radioscopy experimental conditions have been set at a voltage of 40 kV and an electronic current of 2 mA. The exposure time is around a few milliseconds.
A close-up view of the resulting X-ray picture is given in Fig. 5 (left). The honeycomb structure is clearly visible, together with some square artifacts due to pieces of tape pasted on the surface of the skin (of no interest here).

The geometrical properties of the honeycomb core can be retrieved from such pictures. A mesh is extracted manually from the picture (same figure, right), 1D elements corresponding to walls and nodes to wall junctions. The lengths and orientations of each wall are calculated, and walls are grouped as a function of their orientation :

- group 1 : $\theta_i < -35°$
- group 2 : $-35° < \theta_i < 35°$
- group 3 : $\theta_i > 35°$

Resulting distributions of wall groups orientations and lengths are given in Fig. 6. Mean values and standard deviations are given in table 1.

	mean length/std (mm)	mean angle / std (deg.)	mean intensity / std
group 1	3.87/0.32	-53.3/6.2	175/29
group 2	3.64/0.26	5.1/16.7	111/35
group 3	3.84/0.34	53.9/6.6	169/32

Table 1: Mean values of wall lengths, angles and intensities by group. Intensity values are scaled from 0 (black) to 255 (white).

Groups 1 and 3 have similar gaussian-like distributions in terms of orientation and lengths. The relative standard deviation of wall lengths is about 9%, with an orientation standard deviation of about 6 degrees. Group 2 exhibits a different distribution, with an average wall length a bit smaller than groups 1 and 3 (about 0.2mm shorter) and a slightly smaller relative standard deviation (7%). The main difference is observed on the distribution of orientations: the standard deviation of wall orientations is significantly larger for Group 2 (17 degrees, almost 3 times the standard deviation of groups 1 and 3). Moreover, the distribution is visibly asymmetric, and its average value (5.1 degrees) significantly greater than 0 degrees, a value that could have been expected considering that groups 1 and 3 symmetrically distributed around about plus and minus 53 degrees.

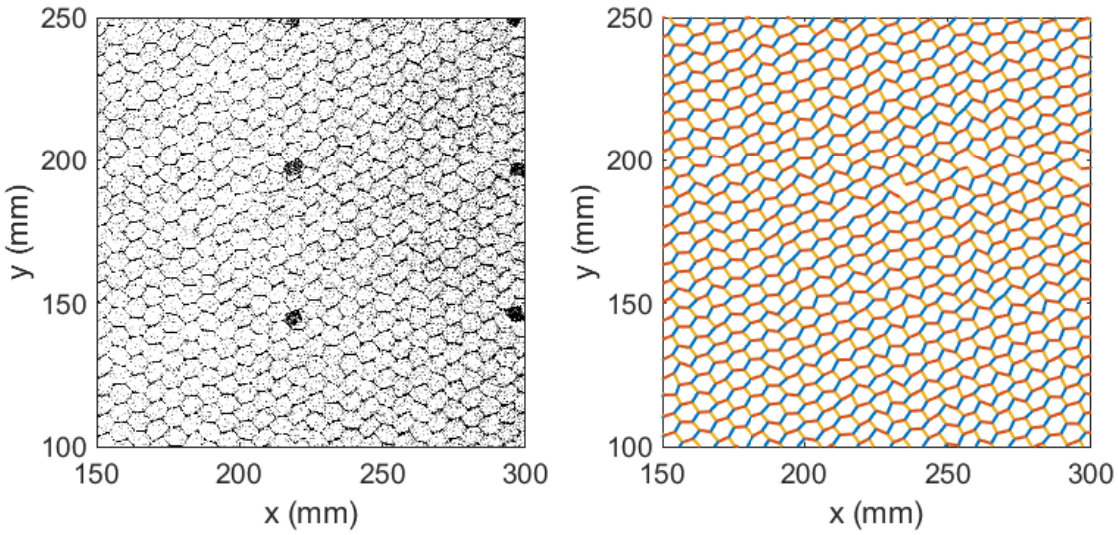

Fig. 5: Left : X-ray picture. Right : extracted mesh. Groups 1, 2, and 3 are drawn in yellow, red and blue, respectively.

It is known that one of the three groups of walls has a doubled thickness due to the manufacturing process. The thickness cannot be precisely estimated from X-ray pictures, because of spatial resolution and parallax issues. However, the image intensity along identified walls is influenced by the thickness of the walls. In order to identify the group of doubled walls, the image intensity is picked up along each edge, and averaged by groups of walls. Resulting average values and standard deviations are reported in table 1. Group # 2 has a significantly lower intensity level (which means significantly darker). This group is thus assumed to be the doubled wall group in the following. This assumption is corroborated by the lengths and orientation distributions, whose shape clearly differs from those of groups #1 and 3. Note that, compared to Figure 3, the structure of the honeycomb is here rotated by 90°.

It is interesting at this stage to have a closer look at the population of unit cells constituting the actual lattice, and their relationship on the homogenised shearing meta-parameters. At each junction, the three connected walls can be used to estimate the values of A, λ and Θ using Eq. (8). This has been done here for the whole honeycomb mesh extracted from X-ray pictures. Resulting shearing parameters are represented using histograms in Fig. 7 (top left, center and right for $A/(G't)$, λ and Θ, respectively). It can be seen that the orthotropy parameter λ takes values over a quite wide range from 0.1 to 0.5. To illustrate this observation, three specific honeycomb cells are selected from the data set for their particularly high, low or regular value of λ (*regular* referring to the regular case studied above with $h = l$, giving $\lambda = 0.25$, see Eq. (13)). These cells are periodized, as shown in the bottom part of Fig. 7. Not surprisingly, the cell with a regular orthotropy has a shape that is very close to the regular cell. The cell with a high orthotropy is particularly skewed, and the corresponding shearing modulus amplitude A is particularly high. This can be explained by the fact that the surface of the skewed cells are smaller than the others, increasing the density of walls (the S_c parameter is at the denominator of $A/(G't)$ in Eq. (13)). The cell with a low orthotropy is characterized by smaller double walls and larger angles for single walls. The study of periodic lattices obtained by periodising a unit cell is interesting to directly relate the shape of the cell to shearing properties. However, the actual lattice is clearly far from a perfectly repeated unit cell, and the variety of cells constituting the actual core of the sample is to be taken into account.

The values of all individual wall lengths and orientations are used in the following to estimate the homogenised shearing properties. The method is similar to the one used in the previous section for a perfect theoretical core, except that instead of summing over wall types as in Eq. (7), the summation is done over the whole set of measured walls, using the geometrical information gathered by the X-ray measurement:

$$G_\alpha = \frac{G't}{S_s} \sum_{i=1}^{N} l_i \beta_i \cos^2(\theta_i - \alpha), \tag{14}$$

where N is the number of walls of the extracted mesh, S_s the sample surface, and β_i a parameter accounting for the

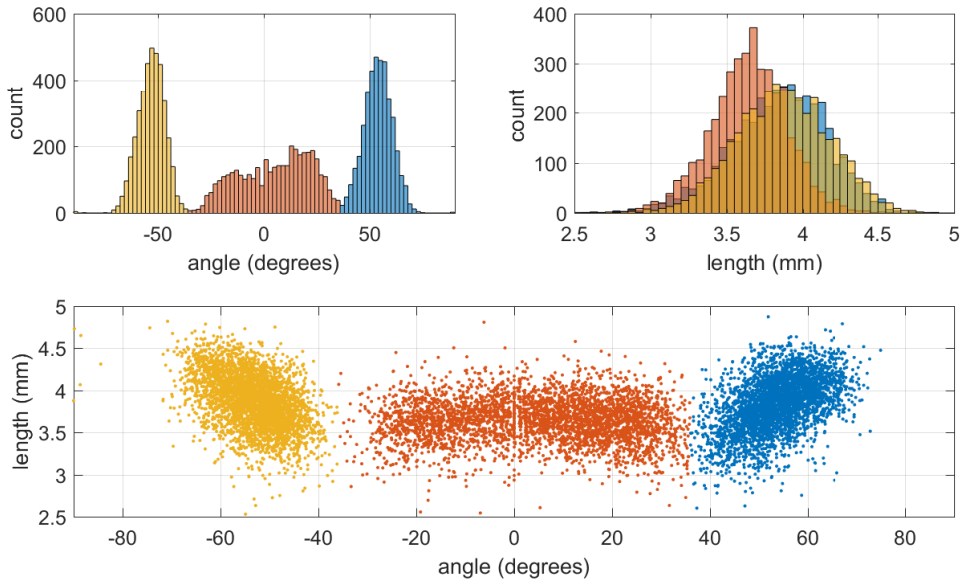

Fig. 6: Distributions of cell wall parameters obtained from the X-ray picture for groups 1, 2, and 3 in yellow, red and blue, respectively.

doubled nature of walls belonging to group 2:

$$\beta_i = 2 \ \forall |\theta_i| \leq 35^\circ, \quad \beta_i = 1 \ \forall |\theta_i| > 35^\circ$$

Note that G_α can also be written in the form $A\left(1 + \lambda \cos\left(2\left(\alpha - \Theta\right)\right)\right)$, with

$$A = \frac{G't}{2S_s} \sum_{i=1}^{N} l_i \beta_i \quad , \quad \lambda = \left| \sum_{i=1}^{N} l_i \beta_i e^{2j\theta_i} \right| / \sum_{i=1}^{N} l_i \beta_i \quad \text{and} \quad \Theta = \frac{1}{2} \arg\left(\sum_{i=1}^{N} l_i \beta_i e^{2j\theta_i} \right). \tag{15}$$

Results obtained from the cell wall lengths and orientations extracted from the X-ray pictures are given in Table 2 (first line).

	$A/(G't)$	λ	Θ
From the full mesh	204 m^{-1}	0.26	8.2°
From the average cell	204 m^{-1}	0.34	7.0°
From the regular cell	204 m^{-1}	0.23	0.0°

Table 2: Meta-parameters of the shearing modulus estimated from the geometric properties of the cell walls.

The parameter A represents the average value of the shearing modulus of the core, it depends on the parameter $G't$ (product of the material shearing modulus by the cell wall thickness). The value of λ is the relative variation of the shearing modulus, whose maximum and minimum values are given by $A(1 \pm \lambda)$. The maximum (resp. minimum) value is obtained for a propagation direction Θ (resp. $\Theta + \pi/2$).

It is interesting to note that the orthotropy angle Θ (8.2°) is significantly different as compared to the average orientation of the doubled walls (group 2, 5.1° according to table 1). In order to understand this result, the contribution of the three wall groups to the shearing modulus as a function of α are drawn in figure 9. The contribution of group 2 reaches indeed a maximum value around $\alpha = 5^\circ$, but is almost constant. The combined contribution of groups 1 and 3, whose orientations are well symmetric (average orientations of $\pm \approx 53^\circ$ according to table 1) is minimum around 0°: it thus increases when receding from zero. The result is that this contribution will always have a tendency to increase the absolute value of the orthotropy angle Θ, thus amplifying the effect of doubled wall orientation.
As it can be seen in table 1, the cell wall parameter distributions have significant variances. In order to assess the effect of these geometrical imperfections on the shearing, a calculation of the shearing is realised based on parameter

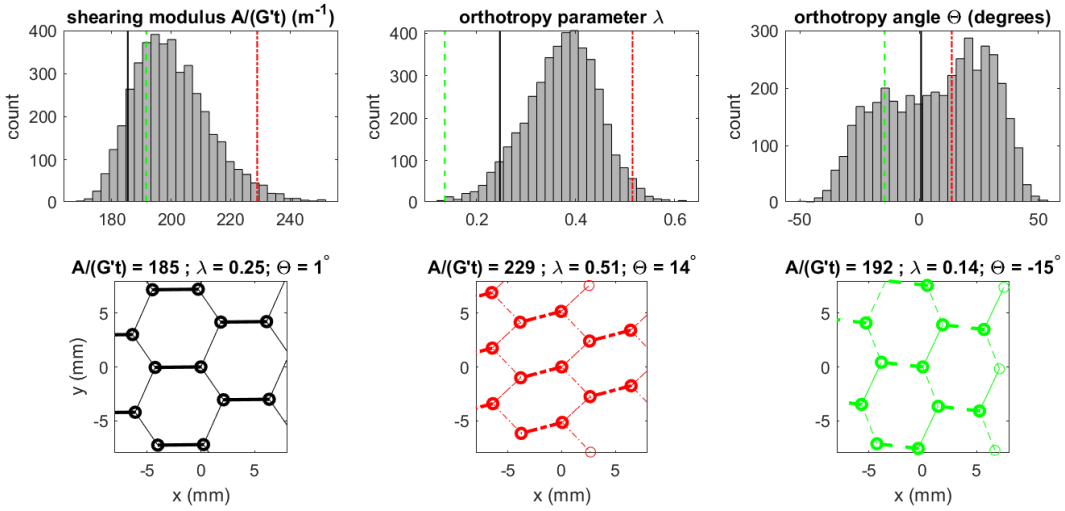

Fig. 7: Top : distributions of shearing parameters estimated from each cell: $A/(G't)$ (left) λ (center) and Θ (right). Bottom: lattices obtained by repeating three honeycomb cells selected from the data set for their particularly regular (left) / high (center) / low (right) orthotropy parameter λ . Doubled walls are indicated by thick lines. The shearing parameters of the three selected cells are shown as vertical lines of the same color on the histograms.

average values, as if the structure was composed of the perfectly repeated average cell:

$$G_\alpha = \hat{A}\left(1 + \hat{\lambda}\cos\left(2\left(\alpha - \hat{\Theta}\right)\right)\right), \tag{16}$$

with

$$\hat{A} = \frac{G't}{2S_c}\sum_{k=1}^{3}\hat{l}_k\beta_k \quad , \quad \hat{\lambda} = \left|\sum_{k=1}^{3}\hat{l}_k\beta_k e^{2j\hat{\theta}_k}\right| \Big/ \sum_{k=1}^{3}\hat{l}_k\beta_k \quad \text{and} \quad \hat{\Theta} = \frac{1}{2}\arg\left(\sum_{k=1}^{3}\hat{l}_k\beta_k e^{2j\hat{\theta}_k}\right).$$

where S_c is the surface of the mean cell, and $\hat{p}$ the average value of the parameter p. Results are given in Table 2 (second line) and also as a function of α in Fig. 8 (dashed line). Note the resulting mean value of the shearing ($\hat{A}$) is the same as the one obtained from the full distributions (A), by definition. The value obtained for ($\hat{\lambda}$) is, however, significantly greater than λ: it means that the variance of the parameters has a tendency to lower the orthotropy of the material. Another interesting point is that the orthotropy angle obtained from the full mesh ($8.2°$ seems to be slightly higher than the one obtained from the averaged cell, $7°$). This is due to the quite strong skewness of the distribution of group 2 wall orientations visible in Fig. 6, with a maximum around 25° for an average of about 5°. Finally, it can be interesting to assess how these results are deviating from the shearing properties of the regular case (regular hexagonal cell, see Fig. 2). Geometrical parameters are taken from table 1 (mean values: $h = 3.64$ mm ; $l = 3.85$ mm ; $\theta = 36.4°$). Meta-parameters A, λ and θ are calculated using Eq. 13, see Table 2 (third line). Note that the orthotropy parameter λ is lowered as compared to the average cell, mainly because of the symmetry assumption of the regular cell.

3 Retrieving the core shearing properties from the dynamic response of the sandwich

3.1 Experimental characterization of the dynamic response of the sandwich structure

The studied honeycomb sandwich panel is studied experimentally using a scanning Laser Doppler Vibrometer (LDV, brand Polytec, type PSV-400). The plate is suspended by means of flexible wires to a frame and centrally excited with a shaker on its backside. The transverse vibration velocity is measured on the frontside of the plate, on a regular mesh of 183×285 points (spatial step 2 mm). The excitation signal is a Gaussian noise bandpass filtered in the studied frequency range 4 to 40 kHz, and used as a reference signal to synchronise velocities measured sequentially in time by the scanning LDV. The real part of the vibration velocity field is drawn at 15 kHz in Figure 10 (left), as well

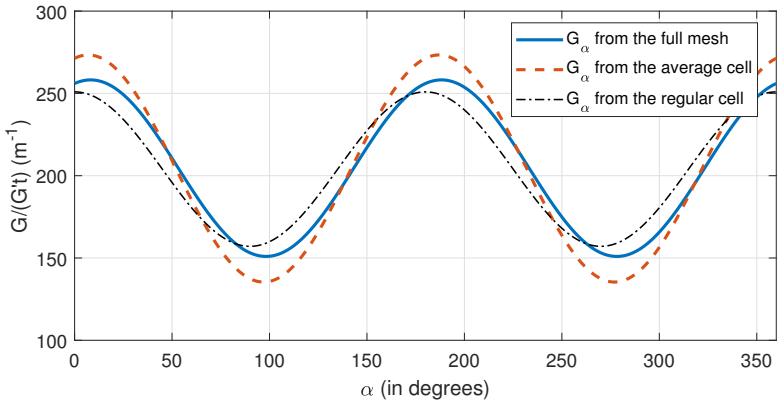

Fig. 8: Shearing modulus of the honeycomb core estimated from the full mesh (Eq. 15), from the average cell (Eq. 16), and from the regular cell (Eq. 13).

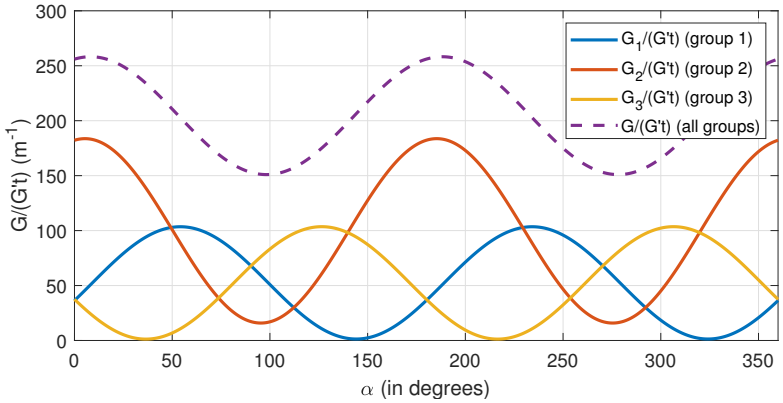

Fig. 9: Shearing modulus of the honeycomb core estimated from the full mesh, and contributions of the three wall families.

as the corresponding wavenumber distribution (squared modulus of the 2D Discrete Fourier Transform, right). This wavenumber representation clearly exhibits an ellipsoidal ridge, confirming the orthotropic nature of the structure.

The principle of wave correlation techniques [39, 11] consists in identifying the natural wavenumber of the structure as the wavenumber maximizing the wavenumber spectrum of a vibration field. When dealing with elliptical orthotropic cases [32], it boils down to an optimisation problem in which the parameters of an ellipse are searched for so as to maximise the wavenumber map averaged along the ellipse. The parameters to be optimized are the semi major and minor axes, as well as the orientation angle. The two first parameters are optimized for each frequency bin, while the orientation angle is assumed to be constant over the frequency. A simple algorithm has been used in this work to solve this optimisation problem, details are provided in an dedicated appendix A.
Results of the optimisation are given in Fig. 11. The fitting score is drawn as a function of the orientation angle (Fig. 11, left). The argument of the maximum of this curve, corresponding to the optimal orientation, is equal to $\hat{\Theta} = 8°$. The optimal values for semi major and minor axes obtained for this particular value of $\hat{\Theta}$ are drawn as a function of the frequency (Fig. 11, right). It corresponds to the natural wavenumbers along the ellipse principal directions, i.e. $\hat{\Theta}$ and $\hat{\Theta} + \pi/2$. It can be seen, at the low frequency range, that both values are very close to one another, implying a quasi-isotropic behavior.

As an illustration, the ellipse curve resulting from this fitting process is drawn in Figure 10 together with the corresponding wavenumber distribution, at the same frequency.

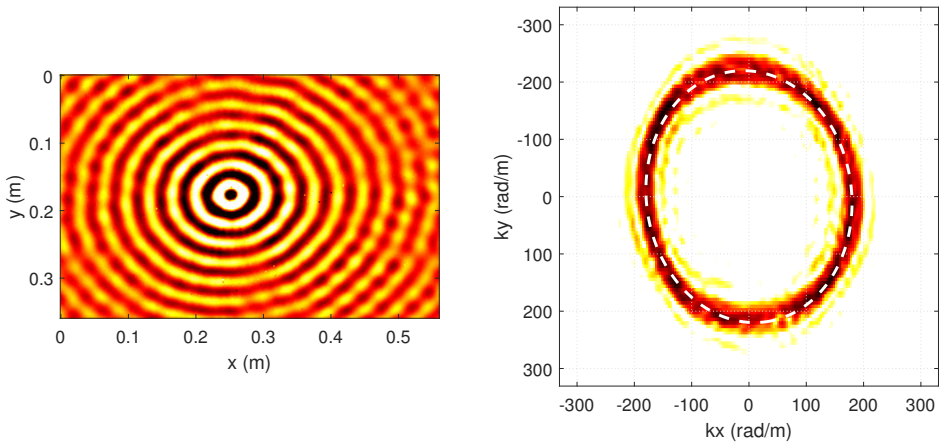

Fig. 10: Vibration velocity field at 15 kHz, real part in the space domain (left), wavenumber distribution (right). Dashed white curve in righ subfigure: ellipse resulting from the fitting procedure.

3.2 Estimation of the core shearing modulus exploiting a dynamic model of the sandwich structure

The core shearing properties estimated from X-ray pictures (section 2.2) can be used as an input for a dynamic model of the sandwich plate, in order to check that the predicted dynamic behavior is in accordance with the observed one. The anisotropic multilayer model proposed by Marchetti [31] is used in this work. The equivalent model describes the bending, membrane and shearing motion of each layer based on Mindlin's theory [40]. Coupling relations between the layers enable to setup the equation of free vibrations of whole multilayer as function of the motion of the first layer only [20, 21, 23, 24]. A plane wave defined by a wavenumber k is used as a specific solution of the equation of motion. Then the system is solved to identify the dispersion curve $k(\omega)$ of the multilayer system [31].

The physical parameters of the studied structure (given in table 3) are used as inputs of the model. Several candidate values for the shearing modulus of the core are considered, ranging from 30 to 150 MPa. The calculated

Aluminum Skins

Thickness h_s	Density ρ_s	Young's modulus E	Poisson's ratio ν
0.6 mm	2700 kg.m^{-3}	70 GPa	0.3

Honeycomb core

Thickness h_c	Density ρ_c	G
9 mm	170 kg.m^{-3}	30 to 150 MPa

Table 3: Elastic properties of the considered sandwich structure

flexural wavenumbers are presented in Figure 12 as a function of frequency. For the sake of readability, wavenumbers are normalized with respect to the asymptotic high frequency flexural wavenumber, when the rigidity of the plate is simply the sum of the rigidities of the skins, as if the shearing modulus of the core was null (see [27] for details):

$$k_{HF}^4 = \frac{\mu}{D_{HF}}\omega^2$$

with μ is the mass per unit area of the sandwich and $D_{HF} = 2Eh_s^3/12/(1-\nu^2)$ (h_s, E and ν standing for the skins thickness, Young's modulus and Poisson's ratio) . The low frequency asymptote of the flexural wavenumber is also plotted in Fig. 12 which corresponds to the thin plate behavior of the whole sandwich (see [27]):

$$k_{LF}^4 = \frac{\mu}{D_{LF}}\omega^2$$

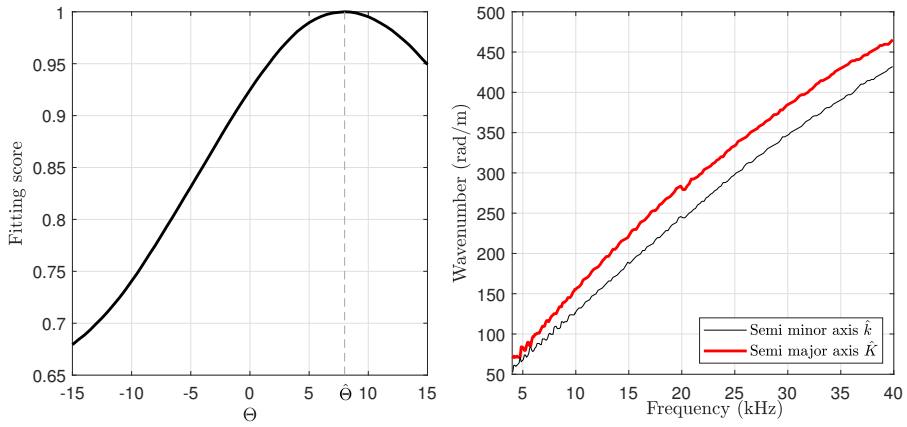

Fig. 11: Left: quantity to be maximized in Eq. A.4 in order to determine $\hat{\Theta}$, Right : optimal values $\{\hat{K}, \hat{k}\}$ (semi-major and minor axes of the ellipse) as a function of the frequency, obtained for $\Theta = \hat{\Theta}$.

where $D_{LF} = E((2h_s + h_c)^3 - h_c^3)/12/(1-\nu^2)$, h_c standing for the thickness of the core.
Calculated wavenumbers nicely tend to approximate values k_{LF} and k_{HF} at very low and high frequency, respectively,

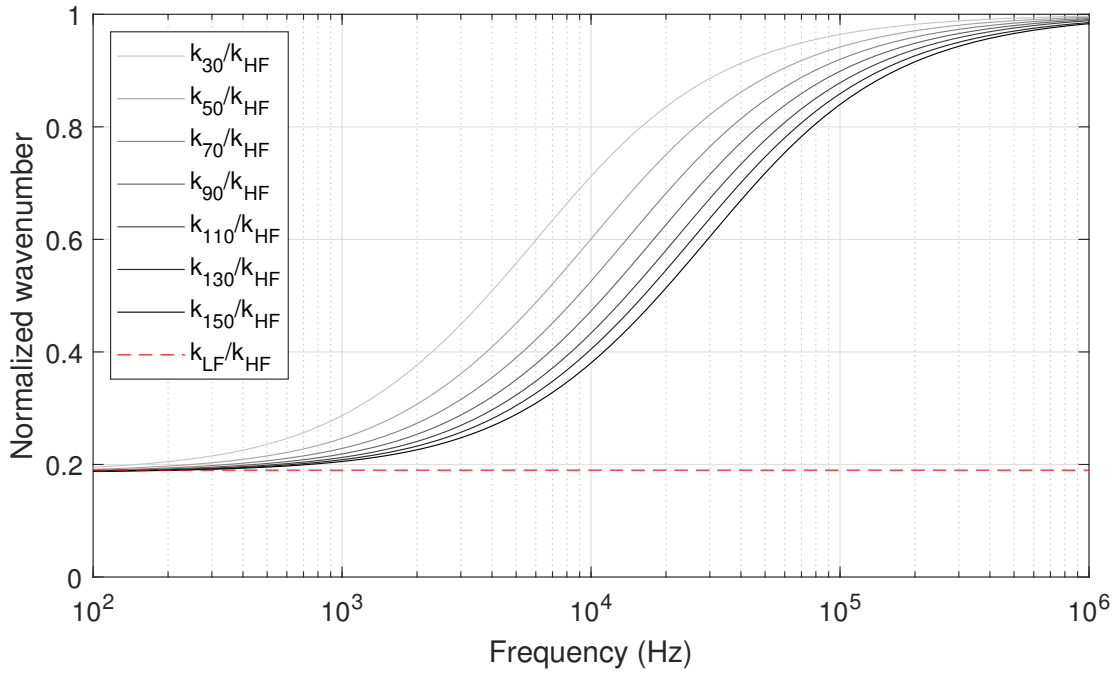

Fig. 12: Wavenumbers computed for various shearing moduli using Marchetti's model [31], normalized by the high frequency flexural wavenumber. k_{XX} stands for the wavenumber obtained for a shearing modulus $G = XX$ MPa.

as expected. Note that in those frequency ranges, the shearing modulus of the core does not affect the flexural wavenumber. In the mid-frequency range, on the contrary, the shearing seem to play a significant part, the transition between LF and HF behavior being slided toward the high frequencies when the shearing modulus increases. These results will be used in the following to identify the effective shearing modulus from the wavenumbers estimated in the previous section.

4 Comparison between shearing properties estimated from X-ray pictures and vibration measurements

4.1 Orthotropy angle

The orthotropy angle obtained from X-ray pictures was 8.2° (see 2). The ellipse fitting procedure conducted from LDV measurements (see section 3 Fig. 11, left) leads to a value of 8.0°, which is in very good agreements with the former result.

4.2 Wavenumber fitting

The shearing modulus of the core used within the modeling approach described in section 3.2 is adjusted so as to superimpose as much as possible the wavenumbers along major and minor axes of the ellipse identified in section 3. This operation allows to identify the value of the core shearing modulus along those two directions. Along the stiffest direction, the core shearing modulus seems to lay around 102 MPa, while its value in the weakest direction would be around 66 MPa. In equation (8), this would place A at 84 MPa and λ at 0.22, which is a bit smaller than the value

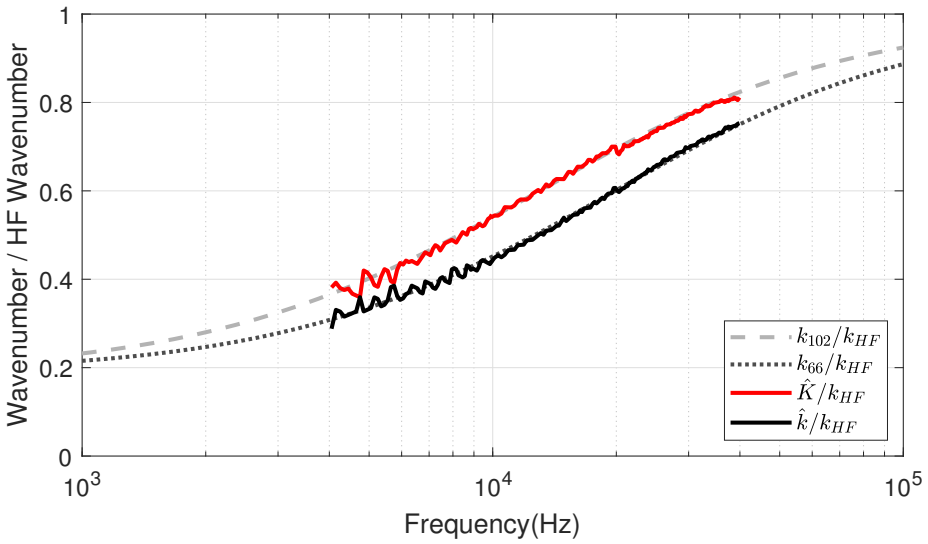

Fig. 13: Wavenumbers along $\hat{\Theta}$ ($\hat{K}$) and $\hat{\Theta}+\pi/2$ ($\hat{k}$) identified from LDV measurements, together with wavenumbers obtained by the Marchetti's model for $G = 102$ MPa and $G = 66$ MPa.

estimated from X-ray pictures ($\lambda = 0.26$).
In section 2.2, according to the analysis of X-ray pictures, a value of 204 m^{-1} was found for the ratio $A/(G't)$. Note that, without the precise knowledge of the core material properties (shearing modulus G' and thickness t), the parameter A remains unknown when considering the geometrical analysis from X-ray pictures only. However, using the value of A estimated from the dynamic analysis, it is possible to assess the $G't$ product so as to verify its order of magnitude. With the value of A equal to 84 MPa, this would situate $G't$ at about 0.41 MPa.m. Kilchert [41] deeply investigated the mechanical properties of resin impregnated aramid paper, constituting the honeycomb core of the studied sample. In his work, the shear modulus was measured using a thick-walled beam shear test ; the resulting shearing modulus was found at 2.3 GPa. This value of shearing modulus would situate the parameter t to 0.18 mm for the sample studied in the present work, which is compatible with X-ray observations: the resolution of X-ray pictures was 0.2 mm, and wall thicknesses occupy roughly on one to two pixels, that could correspond to the thickness of single and doubled walls. However, those values taken for G' and t are very rougth estimates, the purpose here being only to verify that the order of magnitude of the estimated $G't$ product is reasonable.

5 Conclusion

A simple homogenization approach is proposed in this work to understand the shearing behavior of a sandwich structure with a honeycomb core. This approach is versatile enough to be implemented from a theoretical geometry of the hexagonal structure or directly from statistical observations that can be obtained by analysing X-ray pictures. The approach is able to predict the orthotropic nature of the core shearing, particularly the orthotropy angle and amplitude. The dispersion relations were predicted by means of an analytic dynamic model, employing the extracted shearing features of the core. The predicted dispersion relations were compared to dynamic measurements using a Laser Doppler Vibrometer, showing a good comparison. It is shown that the proposed approach is able to predict the orthotropic nature of the core with a satisfying accuracy, enabling an accurate dynamic modelling over a wide frequency range.

Appendix

A Ellipse fitting algorithm

Let's consider an ellipse in the 2D wavenumber plane described by the following parametric equation

$$\begin{aligned} k_x(\theta) &= K\cos\theta\cos\Theta - k\sin\theta\sin\Theta \\ k_y(\theta) &= K\cos\theta\sin\Theta + k\sin\theta\cos\Theta \end{aligned} \tag{A.1}$$

where θ belongs to $[0,\ 2\pi]$, where K and k are the semi-major and minor axes of the ellipse, respectively, and Θ is the angle between the major axis direction and the k_x axis direction.
For a given set of parameters (K, k, Θ), the wavenumber distribution $V[f, k_x, k_y]$ is interpolated on the ellipsoidal parametric curve, and a mean value is calculated integrating the interpolated values over θ :

$$\xi(f,\Theta,K,k) = \int_0^{2\pi} V[f,k_x(\theta),k_y(\theta)]\sqrt{k_x(\theta)^2\cos^2\theta + k_y(\theta)^2\sin^2\theta}\,d\theta \tag{A.2}$$

The resulting score $\xi(f,\Theta,K,k)$ is expected to reach a maximum for the set of parameters (K, k, Θ) describing the natural wavenumber at the frequency f.
Angle Θ is supposed to be constant as a function of the frequency, while K and k are expected to vary. A specific optimization algorithm is thus established as follows :
1) for a given frequency f and angle Θ, find $\tilde{K}$ and $\tilde{k}$ maximizing the fitting score:

$$\{\tilde{K},\tilde{k}\} = \text{argmax}_{K,k}\left(\xi(f,\Theta,K,k)\right) \tag{A.3}$$

2) Determine the optimal angle $\hat{\Theta}$ maximizing the fitting score integrated over a given frequency range:

$$\hat{\Theta} = \text{argmax}_{\Theta}\left(\int \xi(f,\Theta,\tilde{K},\tilde{k})df\right) \tag{A.4}$$

3) Find frequency dependent values of $\hat{K}$ and $\hat{k}$ maximizing the fitting score for the optimal angle $\hat{\Theta}$

$$\{\hat{K},\hat{k}\} = \text{argmax}_{K,k}\left(\xi(f,\hat{\Theta},K,k)\right) \tag{A.5}$$

Authors' Contributions

Q. Leclère is the main contributor to the redaction of the manuscript, and proposed the homogenisation approach based on X-Ray data.
K. Ege contributed to the redaction (main contributor of section 1) and realized the LDV measurements.
F. Marchetti contributed to the redaction (main contributor of section 3.2) and implemented the mutlilayer dynamic model.
N.B. Roozen contributed to the redaction (overviewed the whole paper, contributed to the literature review).
Ph. Duvauchelle, M. Tahraoui and V. Kaftandjian contributed to the redaction (description of the X-Ray measurement setup) and to the X-Ray measurements.
All authors reviewed the final manuscript.

Acknowledgements

This work was performed within the framework of the Labex CeLyA of Université de Lyon, operated by the French National Research Agency (ANR-10-LABX-0060/ ANR-11-IDEX-0007). The authors would like to acknowledge Ms Céleste Leclère for her help in the creation of the mesh from the X-ray pictures.

Supplementary Material

The datasets used in this work are shared publicly on a zenodo repository [42]. Please cite this paper and the reference to the dataset for any subsequent publication exploiting it.

References

[1] S. Kelsey, R. A. Gellatly, and B. W. Clark. The shear modulus of foil honeycomb cores. *Aircraft Engineering and Aerospace Technology*, 30(10):294–302, January 1958. ISSN 0002-2667. doi:10.1108/eb033026.

[2] F. Abd El-Sayed, R. Jones, and I. Burgess. A theoretical approach to the deformation of honeycomb based composite materials. *Composites*, 10(4):209–214, 1979. ISSN 0010-4361. doi:10.1016/0010-4361(79)90021-1.

[3] L. J. Gibson, M. F. Ashby, G. S. Schajer, and C. I. Robertson. The mechanics of two-dimensional cellular materials. *Proceedings of the Royal Society of London. A. Mathematical and Physical Sciences*, 382(1782):25–42, 1982. doi:10.1098/rspa.1982.0087.

[4] L. J. Gibson and M. F. Ashby. *Cellular Solids: Structure and Properties*. Cambridge Solid State Science Series. Cambridge University Press, 2 edition, 1997. doi:10.1017/CBO9781139878326.

[5] K. Renji, P. S. Nair, and S. Narayanan. Modal density of composite honeycomb sandwich panels. *Journal of Sound and Vibration*, 195(5):687–699, 1996. doi:10.1006/jsvi.1996.0456.

[6] T. Saito, R. Parbery, S. Okuno, and S. Kawano. Parameter identification for aluminum honeycomb sandwich panels based on orthotropic timoshenko beam theory. *Journal of Sound and Vibration*, 208(2):271–287, 1997. ISSN 0022-460X. doi:10.1006/jsvi.1997.1189.

[7] W. Burton and A. Noor. Assessment of continuum models for sandwich panel honeycomb cores. *Computer Methods in Applied Mechanics and Engineering*, 145(3):341–360, 1997. ISSN 0045-7825. doi:10.1016/S0045-7825(96)01196-6.

[8] E. Nilsson and A. Nilsson. Prediction and measurement of some properties of sandwich structures with honeycomb and foam cores. *Journal of Sound and Vibration*, 251(3):409 – 430, 2002. doi:10.1006/jsvi.2001.4007.

[9] S. Yu and W. Cleghorn. Free flexural vibration analysis of symmetric honeycomb panels. *Journal of Sound and Vibration*, 284 (1):189–204, 2005. ISSN 0022-460X. doi:10.1016/j.jsv.2004.06.028.

[10] H. Denli and J. Sun. Structural-acoustic optimization of sandwich structures with cellular cores for minimum sound radiation. *Journal of Sound and Vibration*, 301(1):93–105, 2007. ISSN 0022-460X. doi:10.1016/j.jsv.2006.09.025.

[11] M. Ichchou, O. Bareille, and J. Berthaut. Identification of effective sandwich structural properties via an inverse wave approach. *Engineering Structures*, 30(10):2591–2604, 2008. ISSN 0141-0296. doi:10.1016/j.engstruct.2008.02.009.

[12] M. Rébillat and X. Boutillon. Measurement of relevant elastic and damping material properties in sandwich thick plates. *Journal of Sound and Vibration*, 330(25):6098–6121, 2011. ISSN 0022-460X. doi:10.1016/j.jsv.2011.07.015.

[13] R. Cherif, J.-D. Chazot, and N. Atalla. Damping loss factor estimation of two-dimensional orthotropic structures from a displacement field measurement. *Journal of Sound and Vibration*, 356:61 – 71, 2015. doi:10.1016/j.jsv.2015.06.042.

[14] P. Margerit, A. Lebée, J.-F. Caron, K. Ege, and X. Boutillon. The High-Resolution Wavevector Analysis for the characterization of the dynamic response of composite plates. *Journal of Sound and Vibration*, 458:177–196, 2019. doi:10.1016/j.jsv.2019.06.026.

[15] A. Harkati, E. H. Harkati, A. Bezazi, F. Scarpa, and M. Ouisse. Out-of-plane elastic constants of curved cell walls honeycombs. *Composite Structures*, 268:113959, 2021. ISSN 0263-8223. doi:10.1016/j.compstruct.2021.113959.

[16] F. Scarpa and G. Tomlinson. Theoretical characteristics of the vibration of sandwich plates with in-plane negative Poisson's ratio values. *Journal of Sound and Vibration*, 230(1):45–67, FEB 10 2000. ISSN 0022-460X. doi:10.1006/jsvi.1999.2600.

[17] M. Ruzzene, F. Scarpa, and F. Soranna. Wave beaming effects in two-dimensional cellular structures. *Smart Materials and Structures*, 12(3):363–372, JUN 2003. ISSN 0964-1726. doi:10.1088/0964-1726/12/3/307.

[18] F. Scarpa, L. G. Ciffo, and J. R. Yates. Dynamic properties of high structural integrity auxetic open cell foam. *Smart Materials and Structures*, 13(1):49–56, nov 2003. doi:10.1088/0964-1726/13/1/006.

[19] S. Gonella and M. Ruzzene. Analysis of in-plane wave propagation in hexagonal and re-entrant lattices. *Journal of Sound and Vibration*, 312(1):125–139, 2008. ISSN 0022-460X. doi:10.1016/j.jsv.2007.10.033.

[20] J. Guyader and C. Lesueur. Acoustic transmission through orthotropic multilayered plates, part i: Plate vibration modes. *Journal of Sound and Vibration*, 58(1):51–68, 1978. ISSN 0022-460X. doi:10.1016/S0022-460X(78)80060-1.

[21] J. Guyader and C. Lesueur. Acoustic transmission through orthotropic multilayered plates, part ii: Transmission loss. *Journal of Sound and Vibration*, 58(1):69–86, 1978. ISSN 0022-460X. doi:10.1016/S0022-460X(78)80061-3.

[22] E. Carrera. An assessment of mixed and classical theories on global and local response of multilayered orthotropic plates. *Composite Structures*, 50(2):183 – 198, 2000. ISSN 0263-8223. doi:10.1016/S0263-8223(00)00099-4.

[23] J.-L. Guyader and C. Cacciolati. Viscoelastic properties of single layer plate material equivalent to multi-layer composite plate. In *Proceedings of Inter-Noise*, Istanbul, Turkey, August 2007. URL https://www.proceedings.com/03195.html.

[24] J.-L. Guyader, C. Cacciolati, and E. Guyader. Prediction of vibroacoustic behaviour of multilayered structures using equivalent bi-materials. In *Proceedings of Inter-Noise*, Shangai, China, October 2008. URL https://www.proceedings.com/05128.html.

[25] S. Ghinet and N. Atalla. Modeling thick composite laminate and sandwich structures with linear viscoelastic damping. *Computers & Structures*, 89(15):1547–1561, 2011. ISSN 0045-7949. doi:https://doi.org/10.1016/j.compstruc.2010.09.008.

[26] U. Arasan, F. Marchetti, F. Chevillotte, L. Jaouen, D. Chronopoulos, et al. A simple equivalent plate model for dynamic bending stiffness of three-layer sandwich panels with shearing core. *Journal of Sound and Vibration*, 500:116025, 2021. ISSN 0022-460X. doi:https://doi.org/10.1016/j.jsv.2021.116025.

[27] K. Ege, N. B. Roozen, Q. Leclère, and R. G. Rinaldi. Assessment of the apparent bending stiffness and damping of multilayer plates; modelling and experiment. *Journal of Sound and Vibration*, 426:129–149, 2018. ISSN 0022-460X. doi:10.1016/j.jsv.2018.04.013.

[28] M. Gallo, C. Chesnais, K. Ege, Q. Leclère, N. Totaro, et al. Spatial patterning of the viscoelastic core layer of a hybrid sandwich composite material to trigger its vibro-acoustic performances. In *SAE Technical Paper Series*. SAE International, June 2018. doi:10.4271/2018-01-1500.

[29] N. B. Roozen, Q. Leclère, K. Ege, and Y. Gerges. Estimation of plate material properties by means of a complex wavenumber fit using Hankel's functions and the image source method. *Journal of Sound and Vibration*, 390:257–271, 2017. doi:10.1016/j.jsv.2016.11.037.

[30] N. B. Roozen, L. Labelle, Q. Leclère, K. Ege, and S. Alvarado. Non-contact experimental assessment of apparent dynamic stiffness of constrained-layer damping sandwich plates in a broad frequency range using a Nd:YAG pump laser and a laser Doppler vibrometer. *Journal of Sound and Vibration*, 395:90–101, 2017. doi:10.1016/j.jsv.2017.02.012.

[31] F. Marchetti, K. Ege, Q. Leclère, and N. B. Roozen. On the structural dynamics of laminated composite plates and sandwich structures; a new perspective on damping identification. *Journal of Sound and Vibration*, 474:115256, May 2020. doi:10.1016/j.jsv.2020.115256.

[32] F. Marchetti, N. B. Roozen, J. Segers, K. Ege, M. Kersemans, et al. Experimental methodology to assess the dynamic equivalent stiffness properties of elliptical orthotropic plates. *Journal of Sound and Vibration*, 495:115897, March 2021. doi:10.1016/j.jsv.2020.115897.

[33] A. H. Orta, M. Kersemans, N. B. Roozen, and K. Van Den Abeele. Characterization of the full complex-valued stiffness tensor of orthotropic viscoelastic plates using 3d guided wavefield data. *Mechanical Systems and Signal Processing*, 191:110146, 2023. ISSN 0888-3270. doi:10.1016/j.ymssp.2023.110146.

[34] A. Doyum and M. Dürer. Defect characterization of composite honeycomb panels by non-destructive inspection methods. In *Proceeding of conference of German Society of NDT*, Germany, November 2002. URL https://www.ndt.net/search/docs.php3?id=1597.

[35] M. A. Abou-Khousa, A. Ryley, S. Kharkovsky, R. Zoughi, D. Daniels, et al. Comparison of x-ray, millimeter wave, shearography and through-transmission ultrasonic methods for inspection of honeycomb composites. *AIP Conference Proceedings*, 894(1): 999–1006, 2007. doi:10.1063/1.2718076.

[36] D. G. Moore and C. L. Nelson. Damage assessment of composite honeycomb material using advanced inspection technologies. In *Proceeding of conference proposed for presentation at the SAMPE Tech, OSTI.GOV*, United States, July 2012. URL https://www.osti.gov/biblio/1116804.

[37] D. Vavrik, J. Jakubek, I. Jandejsek, I. Kumpova, and J. Zemlicka. X-ray radiography and tomography study of a delamination in a cfrp and honeycomb structures. In *Proceeding of 5th Conference on Industrial Computed Tomography (iCT)*, Austria, February 2014. URL https://www.ndt.net/search/docs.php3?id=15686.

[38] A. Rivera, S. Venkataraman, H. Kim, E. Pineda, and A. Bergan. Finite element modeling for compression strength prediction of honeycomb cores with geometric imperfections measured using X-ray CT imaging. *Proceedings of the American Society for Composites - 37th Technical Conference*, 2022. doi:10.12783/asc37/36497.

[39] J. Berthaut, M. Ichchou, and L. Jezequel. K-space identification of apparent structural behaviour. *Journal of Sound and Vibration*, 280(3):1125–1131, 2005. ISSN 0022-460X. doi:https://doi.org/10.1016/j.jsv.2004.02.044.

[40] R. D. Mindlin. Influence of rotatory inertia and shear on flexural motions of isotropic, elastic plates. *Journal of Applied Mechanics-Transactions of the Asme*, 18(1):31–38, 1951. doi:10.1115/1.4010217.

[41] S. V. Kilchert. *Nonlinear finite element modelling of degradation and failure in folded core composite sandwich structures*. PhD thesis, Universität Stuttgart, 2013, URL https://elib.uni-stuttgart.de/bitstream/11682/3949/1/Dissertation_Kilchert_digital.pdf.

[42] Q. Leclere, K. Ege, M. Tahraoui, and V. Kaftandjian. Ldv and x-ray scans of a honeycomb sandwich panel (dataset). December 2023. doi:10.5281/zenodo.10251364.